





Research Article

Fault Identification of Low-Speed Hub Bearing of Crane Based on MBMD and BP Neural Network

Li-Hong Guo ¹, Lai-Ming Yang ¹, Yan-Feng Peng ², and Yong Guo ²

¹Five Meters Wide Thick Plate Factory, Hunan Hualing Xiangtan Iron and Steel Co., Ltd., Xiangtan 411101, China

²Hunan Provincial Key Laboratory of Health Maintenance for Mechanical Equipment, Hunan University of Science and Technology, Xiangtan 411201, China

Correspondence should be addressed to Li-Hong Guo; xt5mkhb@sina.com

Received 27 May 2022; Accepted 30 June 2022; Published 31 July 2022

Academic Editor: Xingxing Jiang

Copyright © 2022 Li-Hong Guo et al. This is an open access article distributed under the Creative Commons Attribution License, which permits unrestricted use, distribution, and reproduction in any medium, provided the original work is properly cited.

As the key bearing part of the crane, the low-speed hub bearing of the crane exists in special working conditions of low-speed and alternating heavy load. It is difficult to extract its fault characteristics accurately by existing analysis methods. The main idea of the broadband mode decomposition (BMD) method previously proposed is to search in the association dictionary library containing broadband and narrowband signals. However, when it is applied to the broadband signals interfered by strong noise, the decomposition is easy to produce modal confusion, so the modulated broadband mode decomposition (MBMD) method is proposed. The fault signal just can be analyzed by MBMD, so it is applied to the fault diagnosis of low-speed hub bearing of the crane. To realize the fault identification of low-speed hub bearing of the crane, firstly, the original signal is decomposed by MBMD. Secondly, the eigenvalues of the first three-component signals are calculated, the eigenvalue matrix is constructed, and the marked features are selected by the distance evaluation technique (DET). Finally, the marked features are input into BP neural network for training and testing to identify the types of bearing fault. Compared with EEMD, VMD, and BMD, the MBMD method combined with BP neural network has good performance in feature extraction and fault identification.

1. Introduction

Crane is the key core equipment in the field of iron and steel manufacturing; its safe and stable operation and product processing quality greatly affect the normal work and processing cost of steel mills. The low-speed hub bearing of the crane is the key bearing component of the crane, which works in harsh environments and variable working conditions for a long time. Given this, it is necessary to analyze the hub bearing of the crane failure and take targeted preventive measures to ensure that its role and value in industrial production can be fully reflected.

Hub bearing of the crane has the complex operation condition of low-speed and alternating heavy load, which leads to the characteristics of broadband, nonstationary, and strong noise of vibration signal. When the bearing fails, the bearing defect pair usually produces periodic impact on the system, and the impact signal is modulated by the

rotation frequency. Therefore, the bearing fault characteristic frequency band is usually in the form of a narrowband [1]. However, due to low-speed and heavy load, the impact duration of the main bearing of the crane is relatively short, which leads to the short-time impact characteristics of the fault vibration signal. And the frequency spectrum of the short-time impact signal is broadband, which results in the nonstationary characteristics of instantaneous amplitude and instantaneous frequency of bearing vibration signal. At the same time, the hub bearing of the crane carries heavy components such as gear and gear shaft. During the operation of the crane, other components will also become strong alternating vibration sources with the change in working conditions. This large amplitude alternating vibration will form large noise pollution when transmitted to the main bearing, resulting in strong noise characteristics of the hub bearing vibration signal.

In the engineering field, the commonly used time-frequency analysis methods are used to extract fault features from noise interference [2–9]. It can be roughly summarized as ways based on Fourier transform and not based on Fourier transform [10, 11]. The former includes WT and VMD. These methods used for signal decomposition are mainly based on the calculation in the frequency domain. It is proven that VMD shows high accuracy in complex nonstationary signal processing compared with previous methods [12–14]. Non-Fourier transform-based methods, including EEMD, EMD, and LMD, which calculate the envelope of extreme value points, and the vibration signals are separated into several intrinsic modal functions [15]. Xue et al. [16] proposed the EEMD method by mixing diverse degrees of white noise with the original signal and equally sharing the decomposition results. Based on the EMD method, the denoising ability is improved.

For the fault diagnosis of low-speed or heavy-duty bearings, some scholars have carried out relevant research and put forward solutions. Song et al. [17] combined statistical filtering, wavelet packet transform, and motion peak preserving method to extract fault signal features, and they defined frequency domain bearing diagnosis symptom parameters sensitive to bearing fault diagnosis to identify fault types. The experiments verify the effectiveness of the proposed method. In order to effectively extract fault features from low-speed and nonstationary bearing signals, Han et al. proposed a fault feature detection method combining Teager energy operator and complementary ensemble empirical mode decomposition [18]. The results show that this method can effectively extract fault features for fault diagnosis. Jiao et al. [19] solved the wavelet energy spectrum coefficients under different working conditions by wavelet decomposition of acoustic emission signals collected under different working conditions. According to the distribution law of wavelet energy spectrum coefficient under different working conditions, the judgment basis of slewing bearing fault is obtained. Thus, the fault diagnosis of slewing bearing of low-speed and heavy-duty crane is realized. These methods have achieved certain diagnostic results, but they are not fully suitable for the fault identification of low-speed hub bearing. The vibration signal of low-speed hub bearing often presents the characteristics of broadband, nonstationary, and strong noise. The existing fault feature extraction methods, including [20, 21], will inevitably produce errors in the process of broadband signal processing. It is difficult to extract the broadband fault feature information of low-speed hub bearing signal from nonstationary strong noise. The modulated broadband mode decomposition (MBMD) method [22] was previously used for photovoltaic DC signals, which is more suitable for processing nonstationary broadband signals under noise interference. Therefore, this paper uses this method to decompose and denoise the vibration signals of the low-speed hub bearing of the crane and calculates the eigenvalues of the decomposed signals. However, the eigenvalues obtained after signal decomposition are not all conducive to the characterization of the fault characteristics of the low-speed hub bearing. In order to better extract fault features, appropriate feature quantities should be selected to

represent them. The distance evaluation technique (DET) [23] can select features with small intraclass variation and large interclass variation using effective factors. The characteristics corresponding to the effective factors can better distinguish different fault types. Therefore, this paper uses this method to select the eigenvalues calculated after signal decomposition.

The rest of this paper is summarized as follows. The second part introduces the detailed steps of the MBMD algorithm and DET method. In the third part, simulation analysis is carried out to compare the decomposition effects of EEMD, VMD, BMD, and MBMD methods on simulation signals. The fourth part carries on the experimental analysis and combines the four decomposition methods with the BP neural network to identify and compare the fault types of the crane low-speed hub bearing. Conclusions are presented in the end.

2. MBMD and DET

2.1. MBMD Method. Narrowband signals are defined as follows [24]:

$$x_{\text{narrow}}(n) = A(n)\cos(\omega n + \phi(n)), \quad (1)$$

where $\phi(n)$ is a slowly changing function. The frequency band limits $A(n)$, and its center frequency ω' of $A(n)$ is far less than ω . The relative bandwidth is $2\omega'/\omega$, and it is much smaller than 1.

The BMD modulated differential operator given in formula (1) can accurately decompose narrowband signals and noise signals because the modulated differential operator can characterize the flatness of nonstationary signals. And narrowband or wideband signals are invariably more relaxative than noise signals. In the BMD algorithm, a modulated differential operator is constructed; the goal is to ensure that the decomposed components are gentler than the original signal. Even though the modulated differential operator is mainly used to decompose narrowband signals, it is also applicable to wideband signals.

Common pulse signals such as square wave signals and sawtooth wave signals are defined as the broadband signals, mainly because the frequency band of such signals is generally infinite [25]. Their Fourier series are as follows:

$$\text{square}(n) = \sum_{i=1}^{+\infty} \frac{1}{2i-1} \sin[(2i-1)n], \quad (2)$$

$$\text{sawtooth}(n) = \sum_{i=1}^{+\infty} \frac{(-1)^{(i-1)}}{(2i-1)^2} \sin[(2i-1)n]. \quad (3)$$

From equations (2) and (3), the magnitude of the sinusoidal component varies with the frequency. So the construction of broadband signal is as follows:

$$x_{\text{broad}}(n) = \sum_{i=1}^{+\infty} A_i \sin[i\omega n + \theta_i(n)], \quad (4)$$

where A_i reduces with the magnify in ω . When $\omega \rightarrow \infty$, $A \rightarrow 0$ and $\theta(n)$ slowly change.

Even though the frequency of the wideband signal has multiple relationships with the frequency of the narrowband signal in equation (4), the wideband signal still appears more gentle than other signals with a significant reduction of frequency amplitude, which makes it possible to decompose the wideband signal from the strong noise signal. It is worth noting that the original modulated differential operator is designed and served for the accurate decomposition of narrowband signals, so the errors inevitably exist when it is applied to the decomposition of broadband signals. For $x_{\text{narrow}}(n)$, in principle, the resulting signal component is $A \cos(\omega n + \phi(n))$ multiplied by an envelope signal $A(n)/A$, reflected in the narrowband signal having only one main frequency ω .

But in $x_{\text{broad}}(n)$, containing several principal frequencies with different amplitudes such as $A_i \sin[i\omega n + \theta_i(n)]$ and $A_{i-1} \sin[(i+1)\omega n + \theta_{i-1}(n)]$, $A_{i-1} \sin[(i+1)\omega n + \theta_{i-1}(n)]$, the main frequency of a broadband signal is ω . However, the frequency interval between the sinusoidal components is ω , too. The relative bandwidth is equal to the bandwidth divided by the main frequency, which is $\omega/\omega = 1$. In formula (1), we prove that the relative bandwidth of narrowband signals is far smaller than 1. When the broadband signals affected by huge noise are decomposed, the BMD algorithm may regard $A_i \sin[i\omega n + \theta_i(n)]$ and $A_{i-1} \sin[(i+1)\omega n + \theta_{i-1}(n)]$ as two different components due to the insufficient relative bandwidth. In addition, the broadband signal will also be decomposed into some narrowband components.

Now the specific method of how to construct the modulated differential operator will be given.

First, multiply the broadband component signal by the high-frequency sinusoidal signal, as shown in the formula:

$$x'_{\text{broad}}(n) = x_{\text{broad}}(n) \sin(w'n) = \sum_{i=1}^{+\infty} A_i \sin[i\omega n + \theta_i(n)] \sin(w'n). \quad (5)$$

In the equation, $x'_{\text{broad}}(n)$ is a modulated signal, $\sin(w'n)$ is a high-frequency single-frequency signal with $w' = Mw$, and M is a presupposed positive integer. In addition, $x'_{\text{broad}}(n)$ can be converted into the following shape:

$$\begin{aligned} x'_{\text{broad}}(n) &= \frac{1}{2} \sum_{i=1}^{+\infty} A_i \cos[(w' - i\omega)n - \theta_i(n)] \\ &+ \frac{1}{2} \sum_{i=1}^{+\infty} A_i \cos[(w' + i\omega)n - \theta_i(n)]. \end{aligned} \quad (6)$$

The main frequency is shifted from ω to $w' - \omega$ and $w' + \omega$. This leads to the relative bandwidths becoming $w/(w' - \omega)$ and $w/(w' + \omega)$, which are far smaller than 1. It is obvious that when the relative bandwidth of the narrowband signal is modulated by the modulated differential operator, it is also far less than 1. So the modulated differential operator can be constructed as follows:

$$\begin{aligned} T_j &= \|D^{(2)} \text{IMF}_i^j(n)\|_2^2 \\ &+ \lambda \|D^{(2)} [x(n) \sin(w'n) - \text{IMF}_i^j(n)]\|_2^2. \end{aligned} \quad (7)$$

Therefore, the broadband modal decomposition method based on the modulated differential operator is constructed as follows.

According to the meaning of modulated differential operator given in formula (7), the main iterative process of the MBMD method is shown as follows, and the flowchart of this method is introduced in detail in Figure 1.

- (1) Set $r_0(n)$ to be equivalent to $r(n)$.
- (2) Decompose the DC component signal from the original signal.

$$\begin{aligned} \text{IMF}_0(n) &= \text{ifft}[\hat{r}_0(1)], \\ r_1(n) &= x(n) - \text{IMF}_0(n), \end{aligned} \quad (8)$$

where i is set to 1, $\text{fft}[\hat{r}_0(1)]$ is the IFT of $\hat{r}_0(1)$, and $\hat{r}_0(k)$ is the FT of $r_0(n)$.

- (3) The structure of optimization problem P_1 is as follows:

$$\begin{aligned} P_1: & \text{Minimize } T_1(A_1, \omega_1, \theta_1, D_1), T_2(A_2, \omega_2, \theta_2, D_2), \\ & \cdot T_3[(A_3(n), \omega_3(n), \theta_3(n))] \\ \text{ST } x(n) &= \sum_{i=0}^N \text{IMF}_i(n) + \text{res}(n), \text{IMF}_i^j \in \text{Dic}_j, \\ T_j &= \|D^{(2)}[\text{IMF}_i^j(n)]\|_2^2 \\ &+ \lambda \|D^{(2)}[x(n) \sin(w'n) - \text{IMF}_i^j(n)]\|_2^2, \end{aligned} \quad (9)$$

where T_j is the modulated differential operator, and it is given in equation (7), $w' = Mw$, where w is equivalent to the biggest frequency of $r_i(n)$, $\lambda > 0$ can be set to 1, and $D^{(2)}$ is the second-order differential operator.

- (4) Obtain the optimal value T_j ($j = 1, 2, 3$) by solving for P_1 using ACROA, find the minimum value T_j , and select the optimal value $\text{IMF}_i(n)$ of T_j .
- (5) Renew $r_i(n)$: $r_{i+1}(n) = r_i(n) - \text{IMF}_i(n)$.
- (6) If the end condition of formula (10) is met, the iterative process is terminated. Otherwise, go back to Step 3.

$$\frac{\|\text{IMF}_i(n) - \text{IMF}_{i-1}(n)\|_2^2}{\|\text{IMF}_{i-1}(n)\|_2^2} \leq \varepsilon. \quad (10)$$

2.2. DET Method. When the fault of low-speed hub bearing of the crane occurs, the time-frequency domain distribution and amplitude of the signal are quite different from the normal state. At this time, the corresponding spectrum distribution and amplitude will also change. Bearing fault diagnosis often uses statistical parameters in the time domain and frequency domain to characterize fault characteristics [26–29]. The statistical parameters selected in the paper are shown in Table 1.

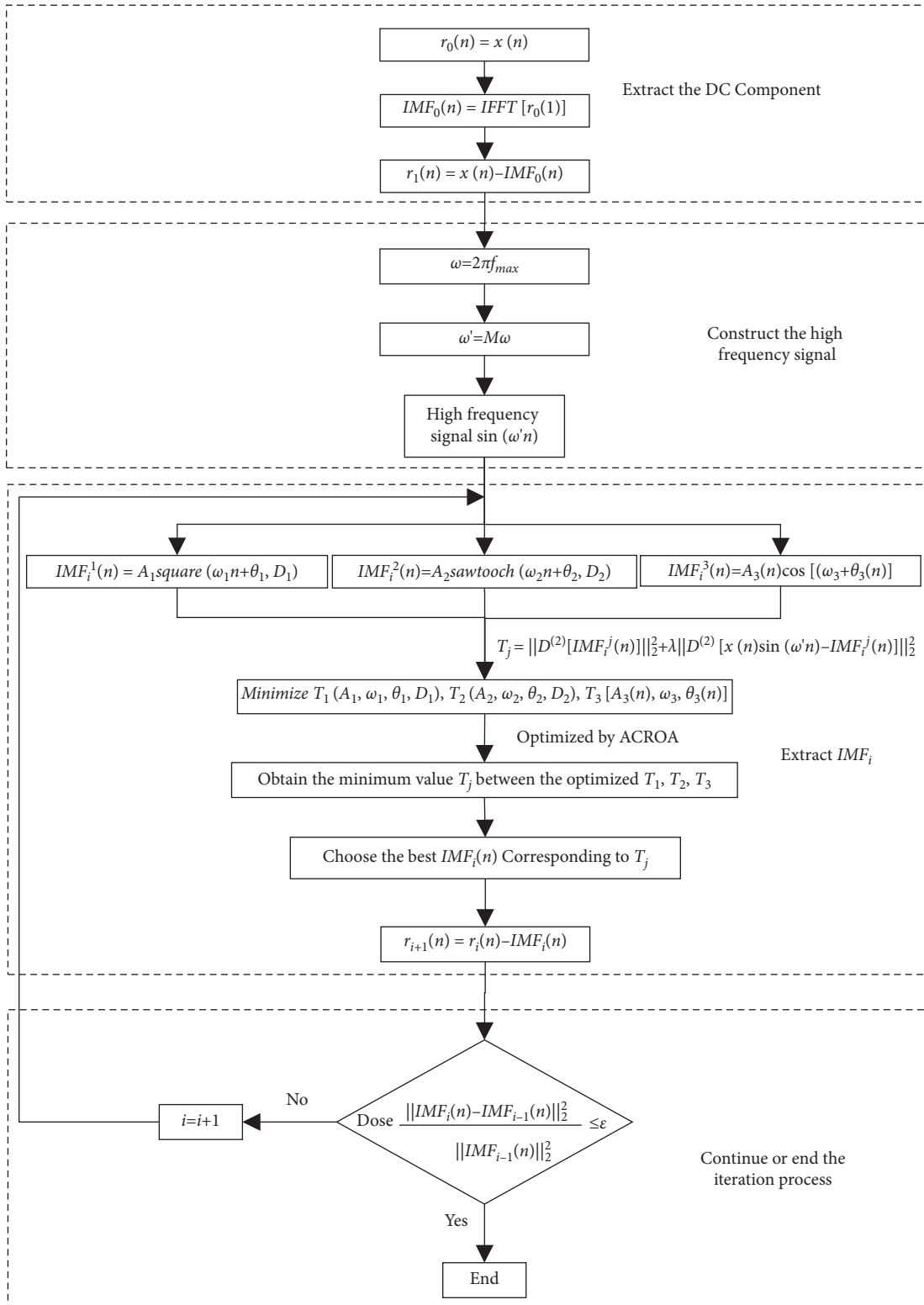


FIGURE 1: The iteration procedure of MBMD.

The MBMD method adaptively decomposes an original signal into a chain of intrinsic mode components, with each IMF representing the inherent vibration modes in the original signal. So features extracted from the IMF are sometimes more efficient than those extracted directly from

the original signal. Although the statistical parameters given in Table 1 can be used to identify the fault types from different angles, not all the characteristics can have a positive effect on the identification of low-speed hub bearing faults of cranes. Some parameters are closely correlated with the

TABLE 1: Time-frequency domain statistical parameters.

Frequency domain statistical parameters		Time-domain statistical parameters	
Mean	Skewness	Spectral amplitude mean	Spectral root 4/2-moment ratio
$p_1 = 1/N \sum_{n=1}^N x(n)$	$p_7 = 1/N - 1 \sum_{n=1}^N x(n) - p_1/p_6$	$p_{13} = 1/M \sum_{k=1}^M s(k)$	$p_{19} = \sqrt{\sum_{k=1}^M f^4(k)s(k) / \sum_{k=1}^M f^2(k)s(k)}$
Root mean square	Kurtosis	Spectral amplitude standard deviation	Spectral standard deviation frequency
$p_2 = \sqrt{1/N \sum_{n=1}^N x^2(n)}$	$p_8 = ((1/N - 1) \sum_{n=1}^N (x(n) - p_1/p_6)^4)$	$p_{14} = \sqrt{1/M - 1 \sum_{k=1}^M (s(k) - p_{13})^2}$	$p_{20} = \sqrt{\sum_{k=1}^M (f(k) - p_{17})^2 s(k) / \sum_{k=1}^M s(k)}$
Square root amplitude	Crest factor	Spectral amplitude skewness	Spectral frequency skewness
$p_3 = (1/N \sum_{n=1}^N \sqrt{ x(n) })^2$	$p_9 = p_5/p_2$	$p_{15} = 1/M - 1 \sum_{k=1}^M (s(k) - p_{13}/p_{14})^3$	$p_{21} = \sum_{k=1}^M (f(k) - p_{17}/p_{20})^3 s(k) / \sum_{j=1}^M s(j)$
Mean amplitude	Clearance factor	Spectral amplitude kurtosis	Spectral frequency kurtosis
$p_4 = 1/N \sum_{n=1}^N x(n) $	$p_{10} = p_5/p_3$	$p_{16} = 1/M - 1 \sum_{k=1}^M (s(k) - p_{13}/p_{14})^4$	$p_{22} = \sum_{k=1}^M (f(k) - p_{17}/p_{20})^4 s(k) / \sum_{j=1}^M s(j)$
Maximum peak	Shape factor	Spectral gravity frequency	
$p_5 = 1/2 (\max(x(n)) - \min(x(n)))$	$p_{11} = p_2/p_4$	$p_{17} = \sum_{k=1}^M f(k)s(k) / \sum_{k=1}^M s(k)$	
Standard deviation	Crest factor	Spectral root mean square frequency	
$p_6 = \sqrt{1/N - 1 \sum_{n=1}^N (x(n) - p_1)^2}$	$p_{12} = p_5/p_4$	$p_{18} = \sqrt{\sum_{k=1}^M f^2(k)s(k) / \sum_{k=1}^M s(k)}$	

Note. $x(n)$ ($n = 1, 2, \dots, N$) is the primary signal, and N is the number of data points. $s(k)$ ($k = 1, 2, \dots, M$) is the amplitude of the original signal spectrum, and M is the number of spectral lines. $f(k)$ is the amplitude of the frequency of the k th spectral line.

faults, while others are not. If all the features are applied to train the classifier, the fault identification precision will be reduced. Therefore, to increase the precision of the classifier, marked features matching the fault information should be selected during the calculation, and irrelevant or redundant features should be removed. In this paper, the distance evaluation technique (DET) method is used to select marked features. The basic idea of the DET method is to select characteristics with small intraclass variation and large interclass variation using effective factors. Features corresponding to effective factors can better distinguish different categories [30, 31]. Set $p_{i,j,k}$ as the j th statistical parameter of the k th sample in the i th category. C and N_i are categories and number of samples, respectively. The effective factor is calculated as follows.

First, calculate the average distance of samples of the same category:

$$d_{i,j} = \frac{1}{N_i(N_i - 1)} \sum_{k,l=1}^{N_i} |p_{i,j,k} - p_{i,j,l}| \quad (k \neq l). \quad (11)$$

Then, get the average distance for all categories:

$$d_j^w = \frac{1}{C} \sum_{i=1}^C d_{i,j}. \quad (12)$$

The mean value of each parameter of the same category sample is as follows:

$$u_{i,j} = \frac{1}{N_i} \sum_{k=1}^{N_i} p_{i,j,k}. \quad (13)$$

The average distance between the mean values of different categories of parameters is shown as follows:

$$d_j^b = \frac{1}{C(C-1)} \sum_{i,m=1}^C |u_{i,j} - u_{m,j}| \quad (i \neq m). \quad (14)$$

Finally, the effective factor is obtained:

$$\alpha_j = \frac{d_j^b}{d_j^w}. \quad (15)$$

To select features, the maximum value is used to normalize the effective factor:

$$\alpha'_j = \frac{\alpha_j}{\max(\{\alpha_j\})}, \quad (16)$$

where α_j is the effective factor of the j th statistical parameter. The upper and lower bounds of the normalized effective factors are 0 and 1. There is no general threshold for the selection of effective factor. In this paper, the normalized effective factor value is set as 0.6, and statistical parameters with an effective factor greater than 0.6 are regarded as marked characteristics. Different marked features have different amplitude ranges, so the normalization of marked feature parameters is shown as follows:

$$f'_{i,j} = \frac{f_{i,j}}{\max_{i=1,2,\dots,l}(\{|f_{i,j}|\})}, \quad (j = 1, 2, \dots, J'), \quad (17)$$

where $f_{i,j}$ is the j th marked parameter of the i th data sample, J' is the number of marked features, and l is the number of samples. $\max_{i=1,2,\dots,l}(\{|f_{i,j}|\})$ is the maximum value of the absolute value of the j th marked parameter for all categories. Formula (16) normalized all marked parameters.

3. Simulation Analysis

To compare the decomposition effects of the different algorithms and to highlight the effectiveness and accuracy of the MBMD algorithm, the BMD, VMD, and EEMD methods are analyzed in comparison with them. First, without loss of generality, the mixed signal shown in the following equation is examined:

$$x(t) = \text{sawtooth}(200t, 0.5) + \cos(8\pi t) \cdot \cos(200\pi t) + n(t), \quad t \in [0, 1]. \quad (18)$$

$x(t)$ given in the formula consists of a sawtooth wave signal, AM-FM signal, and noise signal with a signal-to-noise ratio (SNR) of 10, and the sampling frequency is 12 kHz. The time-domain waveforms of the mixed signal $x(t)$ and its three single components are shown in Figure 2. The MBMD, BMD, VMD, and EEMD methods are used to decompose the mixed signal, respectively, and the decomposition results are taken from the first three components, as shown in Figures 3–6.

As can be seen from Figure 4, when the BMD algorithm decomposes simulation signals, the signals of each component of the mixed signal are not completely decomposed. There are still large noise signals in the component signals, and some errors exist in the decomposition results. This is because when mixed signals are interfered by strong noise, the BMD method may treat sawtooth signals as multiple narrowband components. As can be known from the decomposition results of the MBMD algorithm in Figure 3, the decomposed signals of each component are almost identical to the real components contained in the simulation signals. As for the MBMD algorithm, because the sawtooth signal is modulated by a high-frequency signal, MBMD can obtain more precise decomposition components. The major advantage of the MBMD method over the BMD method is that this method can effectively deal with mixed signals with huge noise or signals relative bandwidth not small enough. Figure 5 shows that when the VMD algorithm decomposes the simulation signal $x(t)$, it has some obvious disturbances in the component signal, and the sawtooth wave signal component has not been decomposed. It can be seen that IMF_2 is the closest to the real component of the AM-FM signal. But the signal component is still disturbed by the noise signal. That is because the thought of the VMD method is adaptive filtering. Figure 6 is the result of the decomposition of the

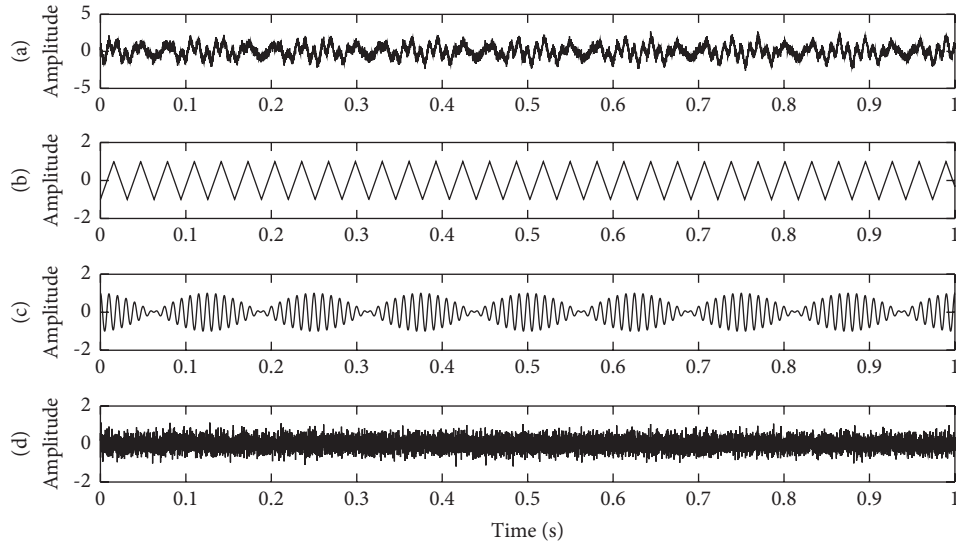


FIGURE 2: The time-domain waveforms of $x(t)$ and the three components. (a) Mixed signal (SNR = 10); (b) sawtooth wave signal; (c) AM-FM signal; (d) noise signal.

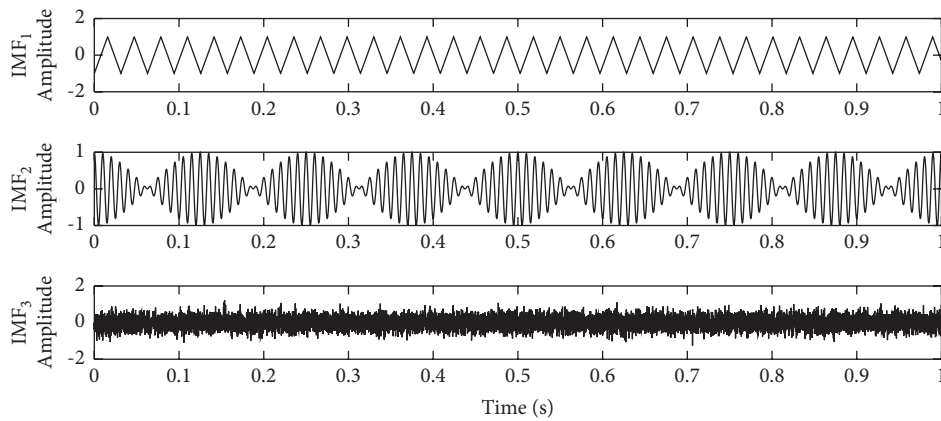


FIGURE 3: The decomposition result of $x(t)$ generated by MBMD.

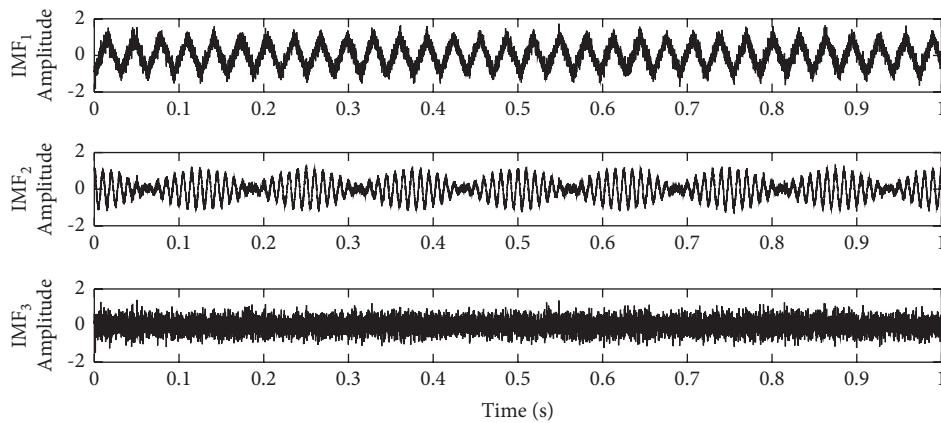


FIGURE 4: The decomposition result of $x(t)$ generated by BMD.

original signal by using the EEMD algorithm. Obviously, there is a large error in the obtained decomposition component signal, and the sawtooth wave signal is not

decomposed but mixed in the original simulation signal. Moreover, the AM-FM component signal has been completely submerged by noise and has not been decomposed.

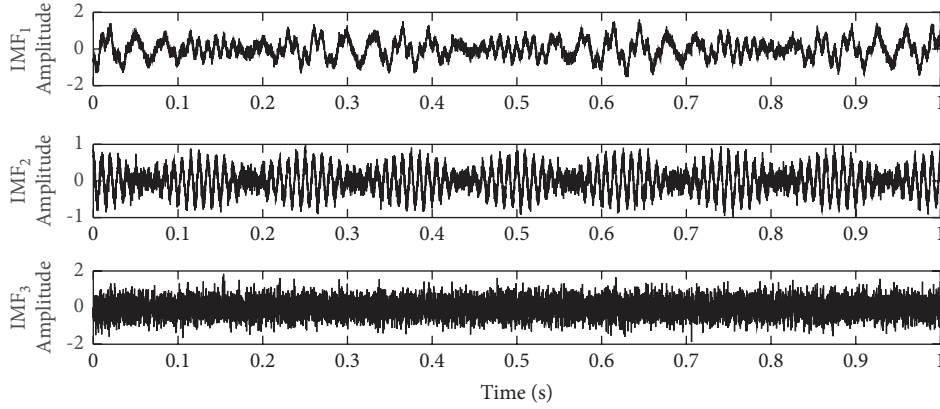


FIGURE 5: The decomposition result of $x(t)$ generated by VMD.

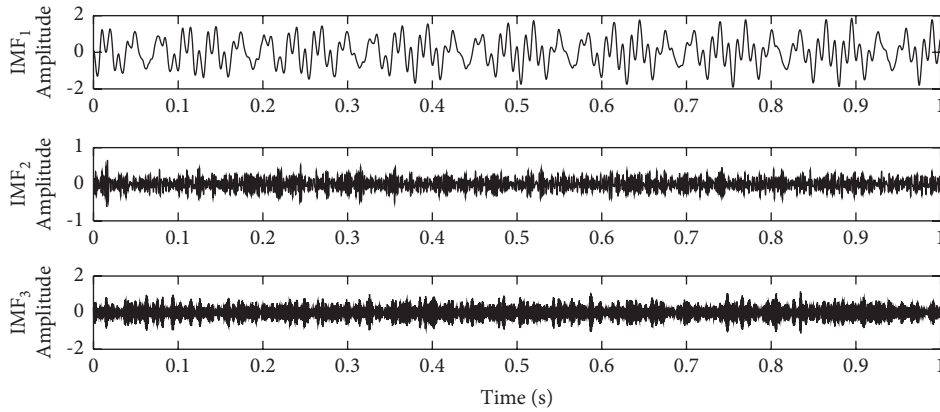


FIGURE 6: The decomposition result of $x(t)$ generated by EEMD.

This is because EEMD uses interpolation methods to get the extreme value point envelope. This will come into being the gentle IMF components.

For a more precise comparison, Table 2 gives the precision parameters of IMF decomposition gained by four methods, including the energy error E_i , correlation coefficient r_i , and time T , where r_i and E_i are the comparison results between the i th actual component obtained by decomposition and its corresponding decomposed component. Meanwhile, for the sake of comparing the computation time of different decomposition methods, the decomposition process is performed on the same computer. The analysis results in Table 2 once again show that the MBMD algorithm can obtain signal components that are closer to the actual signal, with the smallest error of decomposition and more precise decomposition results. However, because of the complex optimization program, the MBMD algorithm will take more computing time than the other three methods.

4. Experimental Analysis

4.1. Experimental Equipment and Data Acquisition. In this paper, the low-speed hub bearing of the crane on the production line of steel companies is used as a research object, and its fault identification is carried out. The analysis

TABLE 2: Evaluation parameters of decomposition accuracy.

Method	r_1	E_1	T (s)
MBMD	0.9921	0.0025	23.2473
BMD	0.8863	0.1591	16.4287
VMD	0.7549	0.2827	10.5492
EEMD	0.5024	0.5283	5.9216

data came from low-speed hub bearing vibration signals collected in the laboratory, and Figure 7 is the fault test bench. The test bench consists of an acceleration sensor, experimental bearing, load pressurization device, coupling, gearbox, alternating current motor, and signal acquisition system. The supporting shaft is driven by the motor, and the rotation rate is determined by the alternating current drive. The speed working condition can be set by adjusting the frequency converter indicator. Two low-speed hub bearings are installed on the support shaft, with the healthy bearing on the left and the experimental bearing on the right for setting different fault types of bearings. The load state of the experimental bearing is set by pressing the pressure handle, and an acceleration sensor is placed on the shell of the experimental bearing to collect vibration signals.

During the experiment, the sampling frequency was set to 1 kHz, and for each group of experiment data, the sampling time is 10 minutes. Before the start of the experiment, the acceleration sensor was installed on the bearing

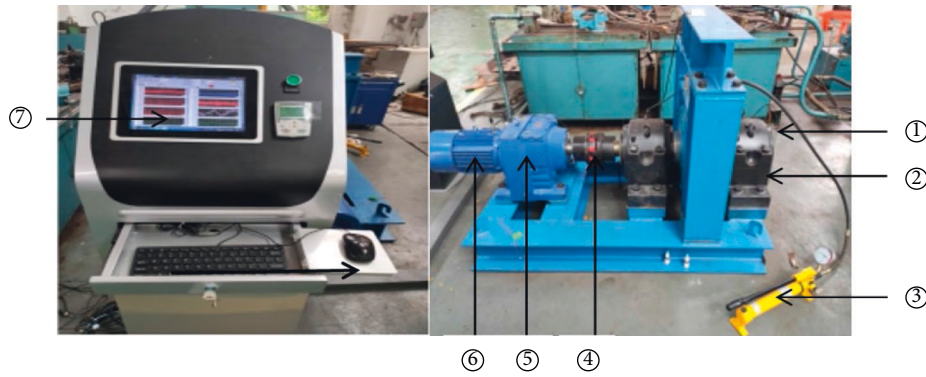


FIGURE 7: Fault test bench. ① Acceleration sensor. ② Experimental bearing. ③ Load pressurizing device. ④ Coupling. ⑤ Gearbox. ⑥ 3 kW AC motor. ⑦ Signal acquisition system.

seat, and the load pressure on the bearing was set to 25 MPa. Since the low-speed hub bearing of the crane in the steel mill mainly works at 38 r/min, the bearing speed is treated similarly in the experiment. Before each group of data collection, the experimental bearings with different fault states that had been set in advance were replaced. Finally, three groups of experimental data were taken under normal state, inner race fault, and outer race fault, respectively, for experimental analysis. The relevant parameters of low-speed hub bearing of the crane are shown in Table 3. According to the known conditions in the table and the theoretical formula calculation, fault characteristic frequencies of inner race, outer race, rolling element, and cage, respectively, are 6.84 Hz, 5.19 Hz, 2.22 Hz, and 0.27 Hz.

4.2. Signal Decomposition and Denoising Analysis. Firstly, MBMD, BMD, VMD, and EEMD methods are used to decompose a total of 90 experimental signals in three states to extract fault characteristic information. Figures 8–11 show the decomposition results of a randomly selected set of samples in class 3 outer race fault data using four methods.

Compared with the decomposition diagrams, it can be seen that the components decomposed by the MBMD method are more stable, and the decomposition results are relatively more accurate. In addition, the vibration signal collected during the experiment contains a lot of noise interference. Therefore, in order to illustrate the denoising effect of the decomposition method adopted in this paper, we compare and analyze the vibration signal with noise in the experiment part. Generally speaking, the better the denoising effect of the vibration signal, the clearer its envelope spectrum. Therefore, we choose the first signal component decomposed by MBMD, BMD, VMD, and EEMD methods for envelope spectrum analysis. The specific results are shown in Figures 12–16.

Comparing the envelope spectrum of the experimental signal finally obtained by the above different decomposition methods, we can see that the relative frequencies in the envelope spectrum of the original signal are mainly modulated by the rotation frequency, while the fault frequencies are covered by a large number of noise signals and are not obvious. In the envelope spectrum obtained after decomposing

the vibration signal by the MBMD method, the valuable frequency information is mainly concentrated in the low-frequency band, and the envelope spectrum is also relatively clear, which achieves a good denoising effect. In the envelope spectrum obtained after decomposing the vibration signal by BMD and VMD methods, there are different degrees of noise interference, resulting in the drowning of important frequency information in the low-frequency band. At the same time, from the envelope spectrum obtained after decomposing the vibration signal by the EEMD method, it can be seen that the denoising effect of this method is not obvious, and the envelope spectrum is similar to the original signal without denoising. Therefore, through the analysis of the vibration signal with noise, we can find that the MBMD method adopted in this paper can denoise effectively.

4.3. Fault Identification of Low-Speed Hub Bearing of Crane.

The vibration signals of the experimental bearing in the three states of normal, inner ring fault, and outer ring fault are selected for fault identification of the low-speed hub bearing of the crane. Firstly, the signals of experimental bearing in three health states under the same speed and load conditions were intercepted at equal times, and the vibration signals of each state were equally divided into 30 groups. The detailed introduction of the experimental data set is shown in Table 4; that is, the data set in Table 4 contains three states of experimental bearing, and each state contains 30 samples.

To prove the validity of the method used, the paper contrasts the four algorithms of MBMD, BMD, VMD, and EEMD, combined with the DET method for the extraction of fault characteristics of the experimental signals of low-speed hub bearing of crane, and uses BP neural network for fault identification. To begin with, we set the hyperparameter of the BP neural network. The detailed settings are as follows. Sigmoid function is selected as the activation function. Three layers are selected for the number of network layers, including input layer, hidden layer, and output layer. Since the experimental data includes three healthy states of normal, inner race fault, and outer race fault, the number of neurons in each layer is determined to be 3, 7, and 3. The initialized weights of the input layer are all set to 0.1, 0.1, 0.2, 0.2, 0.2, 0.1, and 0.1. The learning rate

TABLE 3: Experimental bearing data parameters.

Bearing type	Pitch diameter	Ball diameter	Number of balls	Contact angle
SKF22238-MB	265 (mm)	37 (mm)	19	10°

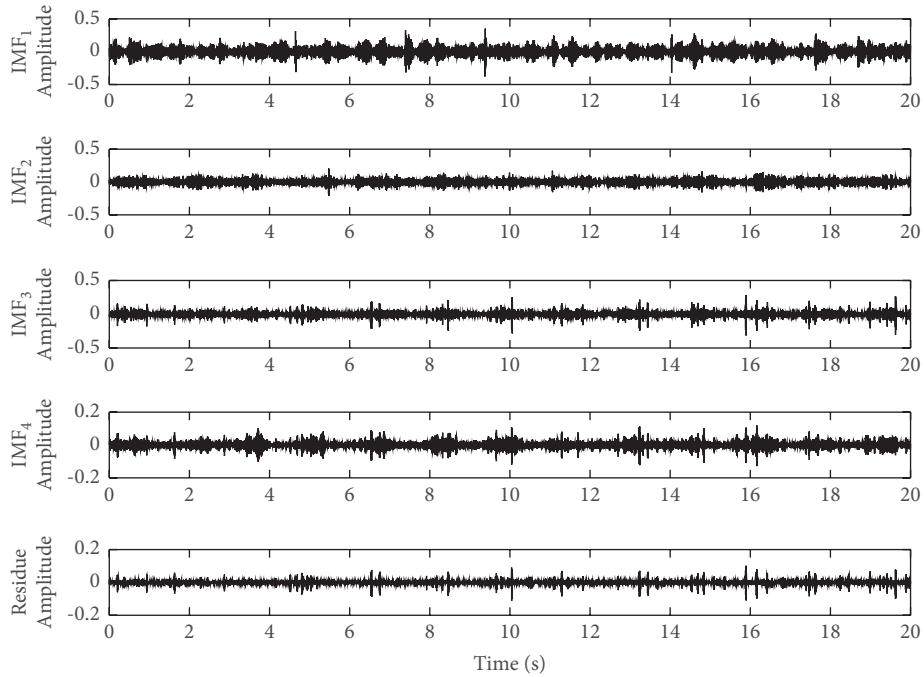


FIGURE 8: The decomposition results generated by MBMD of a vibration signal from class 3.

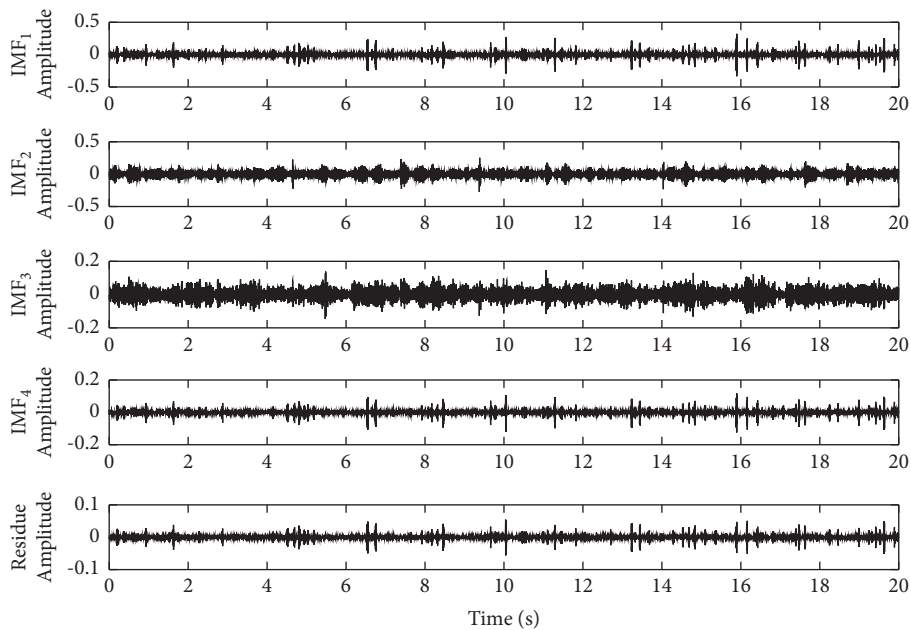


FIGURE 9: The decomposition results generated by BMD of a vibration signal from class 3.

is set to 0.1. The target error for iteration termination is set to 10^{-6} .

Although the statistical parameters given in Table 1 can be featured from different angles for fault types, most of the vibration signals are interfered by noise signals. Therefore,

for the sake of improving the recognition accuracy of the classifier, it is required to select marked features matching the fault information and remove irrelevant or redundant features during the calculation. Therefore, this paper combines the DET method to select marked features for the

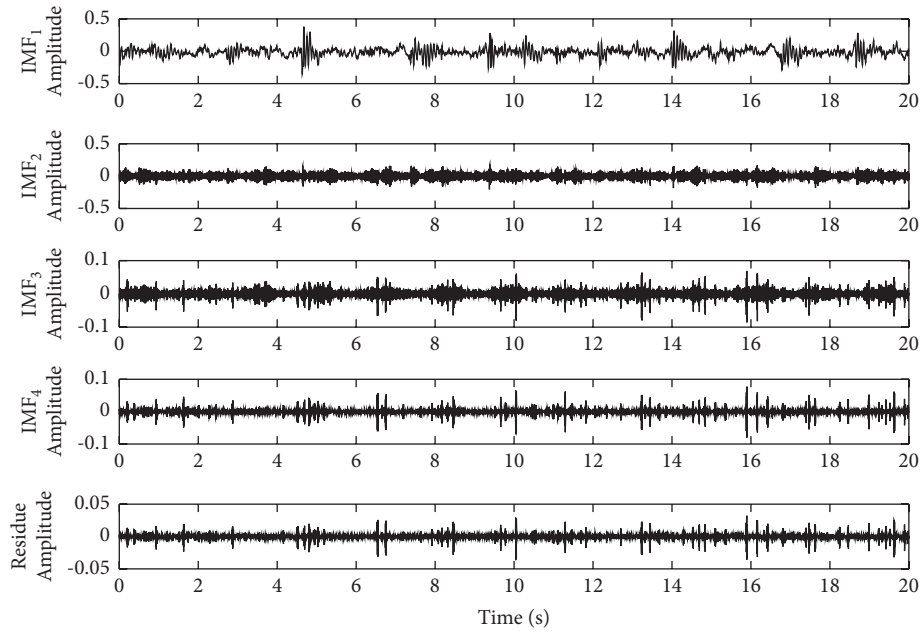


FIGURE 10: The decomposition results generated by VMD of a vibration signal from class 3.

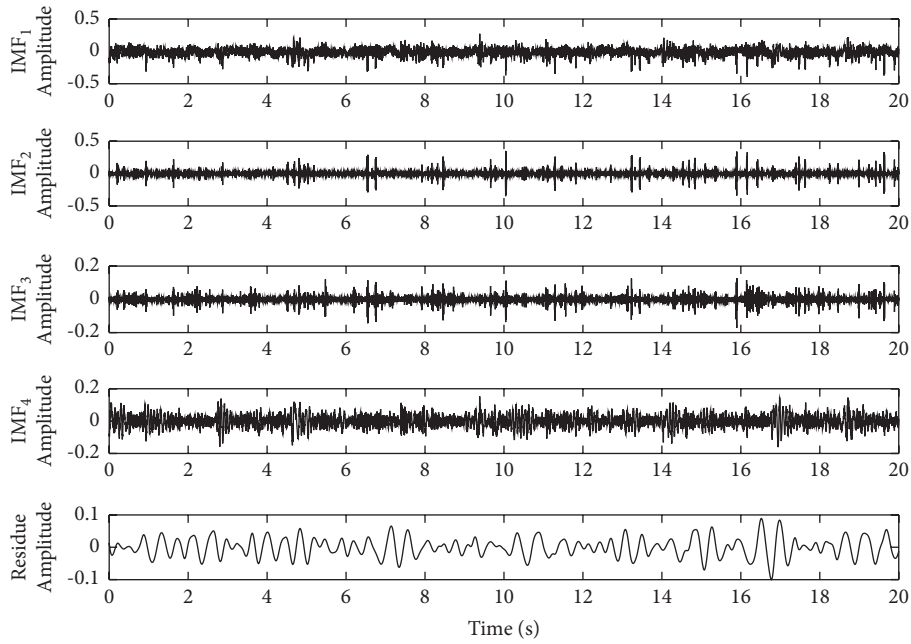


FIGURE 11: The decomposition results generated by EEMD of a vibration signal from class 3.

characteristic values obtained in Table 1. Finally, the obtained marked features are input into BP neural network for training and testing, and the recognition effects are compared. The specific steps of the low-speed hub bearing fault identification method are as shown as follows:

- (1) The original signals of the experimental bearings in three states are decomposed to obtain a series of signal components IMFs.
- (2) All the eigenvalues (22 time-frequency domain statistical parameters in Table 1) are calculated by taking the first three IMFs components as eigenvalue vectors, so there are 66 eigenvalues in each group of signals.
- (3) Get the normalized eigenvalue vector $\alpha'_j (j = 1, 2, \dots, 66)$. DET method is used for feature selection, and features with normalized effective factor value greater than 0.6 are selected as marked features.

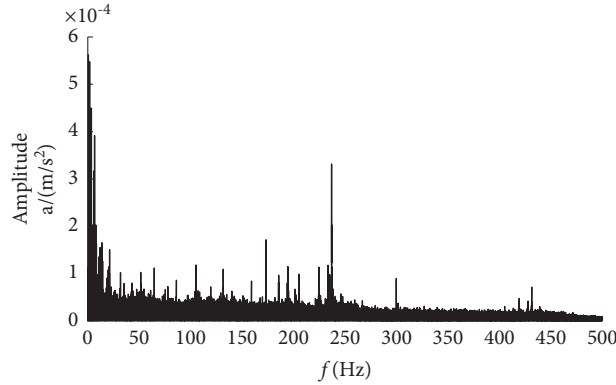


FIGURE 12: The envelope spectrum of the raw signal of a vibration signal from class 3.

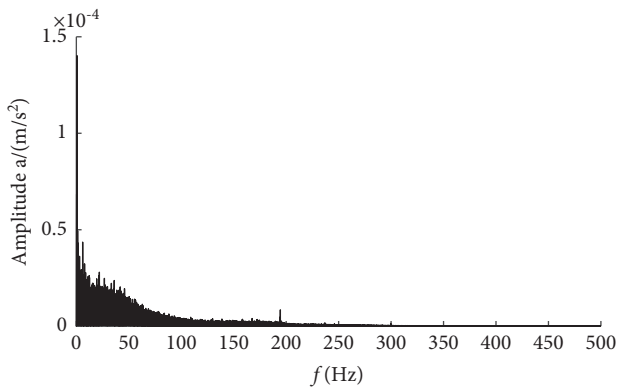


FIGURE 13: The envelope spectrum of the first component derived from MBMD decomposition of a vibration signal from class 3.

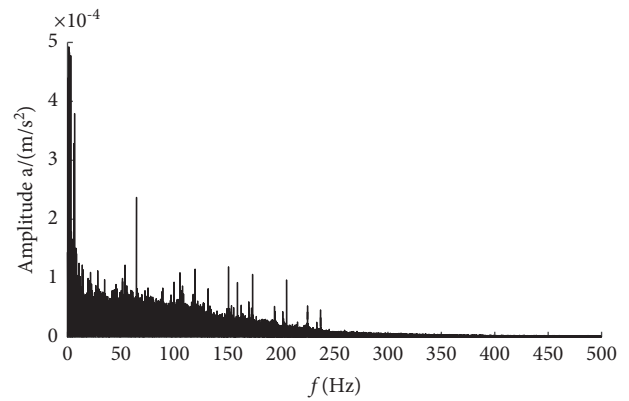


FIGURE 15: The envelope spectrum of the first component derived from VMD decomposition of a vibration signal from class 3.

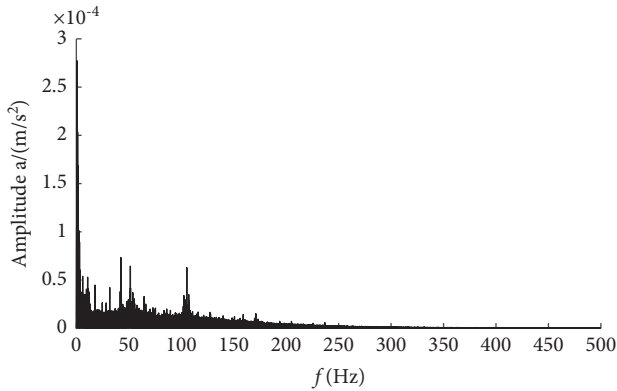


FIGURE 14: The envelope spectrum of the first component derived from BMD decomposition of a vibration signal from class 3.

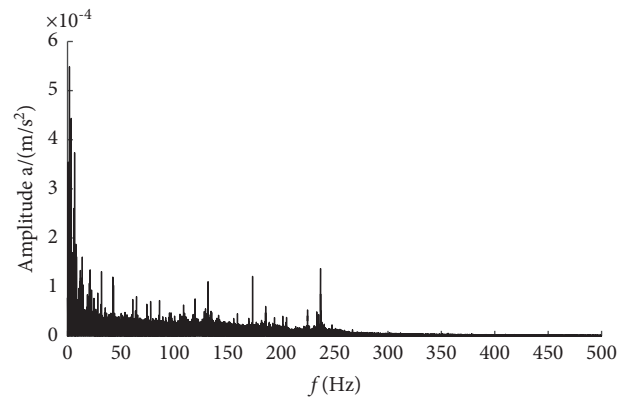


FIGURE 16: The envelope spectrum of the first component derived from EEMD decomposition of a vibration signal from class 3.

- (4) BP neural network is used to train and test the marked features and realize the identification and classification of low-speed hub bearing fault types.

In order to analyze and compare, in each of the 30 sets of data in the three healthy states, 20 sets of data are randomly determined for training, and the rest 10 sets of data are served as test samples, that is, a total of 60 groups of training samples and 30 groups of test samples. Four decomposition methods are used in the experiment and combined with the

DET method to screen the eigenvalue matrix for marked features, and the selection of salient features is shown in Figures 17–20 (the salient features are marked with blue circles). It can be seen that EEMD decomposition combined with DET method finally obtained 9 marked features, VMD decomposition combined with DET method finally obtained 15 marked features, BMD decomposition combined with DET method finally obtained 24 marked features, and MBMD decomposition combined with DET method finally obtained 32 marked features, indicating that the MBMD

TABLE 4: Experimental data set.

Fault class	Number of data sets	Class label
Normal	30	1
Inner race fault	30	2
Outer race fault	30	3

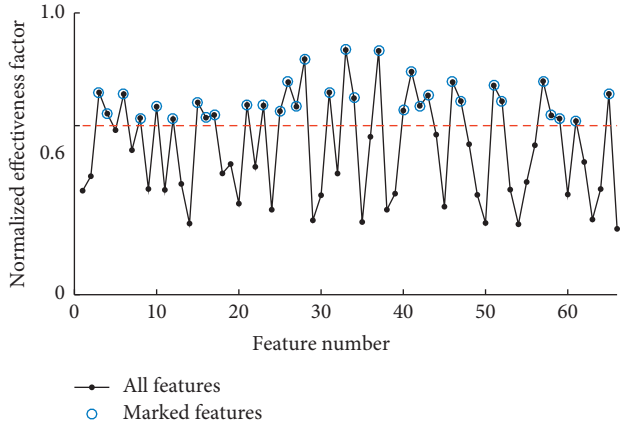


FIGURE 17: The marked features of IMFs components derived from MBMD decomposition.

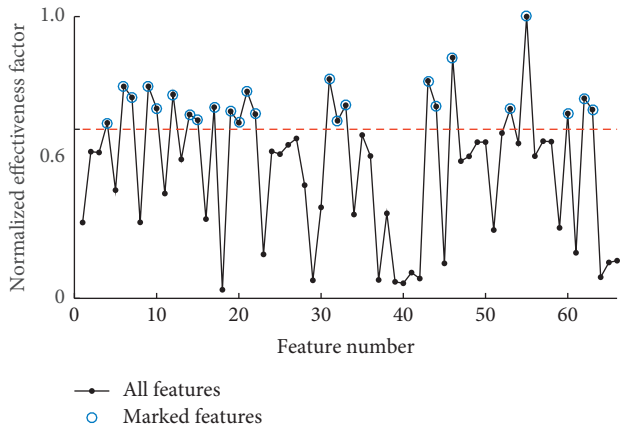


FIGURE 18: The marked features of IMFs components derived from BMD decomposition.

method combined with DET can extract more fault characteristic information. The identification effects of the BP neural network for test samples are shown in Figure 21. As can be known from the identification figure, the identification results obtained by combining EEMD and VMD methods with BP neural network have many errors, among which there are 12 errors in the identification results of EEMD-BP and 9 errors in the identification results of VMD-BP. There are 5 classification errors in BMD-BP identification results, while in the identification results of test samples obtained by MBMD-BP, only 1 case of misclassification occurred in state 2, while other states are accurately classified, with a total accuracy of 96.67%. Table 5 shows the specific classification obtained by four decomposition methods combined with the BP neural network, indicating

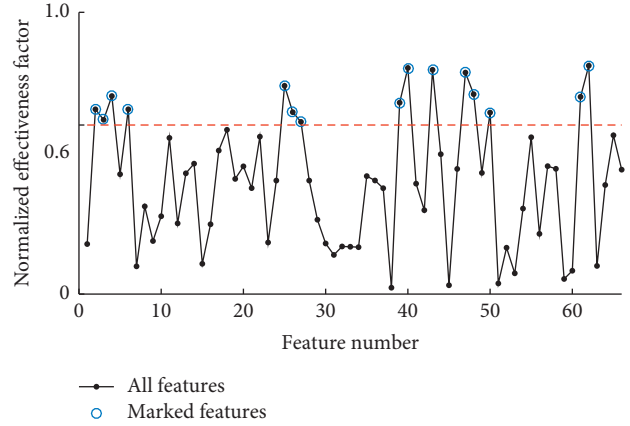


FIGURE 19: The marked features of IMFs components derived from VMD decomposition.

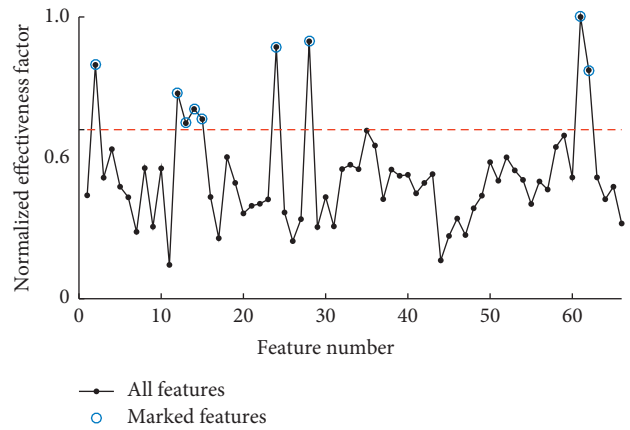


FIGURE 20: The marked features of IMFs components derived from EEMD decomposition.

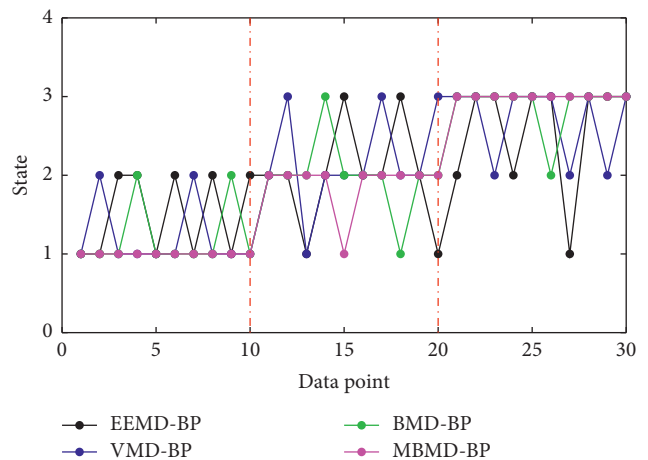


FIGURE 21: Fault identification diagram of low-speed hub bearing of the crane.

that the MBMD-BP method can identify the fault types of low-speed hub bearing of the crane more accurately and effectively. However, the time required by this method for classification and recognition is significantly higher than the

TABLE 5: The identification accuracy of four decomposition methods combined with the BP neural network.

Method	Correct number	Wrong number	Accuracy rate	Time (s)
EEMD-BP	18	12	60%	4.35
VMD-BP	21	9	70%	9.52
BMD-BP	25	5	83.33%	16.87
MBMD-BP	29	1	96.67%	25.63

other three methods, which is mainly related to the complex internal optimization of the MBMD method when decomposing vibration signals.

5. Conclusion

Low-speed hub bearing, as the key bearing component of the crane, is prone to different types of faults in special working environments such as low speed and complex alternating heavy load. To solve this problem, the BMD method is combined with a modulation differential operator; that is, the MBMD method is used to process vibration signals. By decomposing the vibration signals of low-speed hub bearing of crane, using the DET method to screen the marked features of the calculated eigenvalue matrix, combined with the BP neural network, the accurate identification of fault types of low-speed hub bearing of crane is realized.

- (1) Aiming at the difficulties of fault features extraction under the influence of noise on low-speed hub bearing of crane, the modulated broadband mode decomposition (MBMD) method is adopted. The MBMD method is compared with EEMD, VMD, and BMD methods. And the simulation analysis shows that the MBMD method has good decomposition precision, is superior to EEMD, VMD, and BMD methods in suppressing mode aliasing, orthogonality, and anti-noise performance, and can accurately extract the effective components of mixed signals.
- (2) MBMD method combined with BP neural network is applied to identify the fault types of low-speed hub bearing of the crane. Experimental analysis shows that the MBMD method is better than EEMD, VMD, and BMD in extracting fault features accurately, and the DET method can screen out more representative marked features from vibration signals. The MBMD method combined with BP neural network shows good performance in identifying fault types of low-speed hub bearing of the crane and can achieve high identification accuracy.

Of course, the MBMD method also has some shortcomings. For example, the internal optimization process of the MBMD method is complicated, the calculation time will be relatively long, and so on. Therefore, we will conduct more in-depth research and improvement on these problems in the future.

Data Availability

The data used to support the findings of this study are available from the corresponding author upon request (e-mail: xt5mkhb@sina.com).

Conflicts of Interest

The authors declare that they have no conflicts of interest.

Acknowledgments

This work was supported by the Major Science and Technology Project of Hunan Province under Grant no. 2021GK1070 and the Hunan Provincial Natural Science Foundation of China under Grant no. 2021JJ30260.

References

- [1] J. Duan, T. Shi, H. Zhou, J. Zhang, and Y. Zhang, "Multiband envelope spectra extraction for fault diagnosis of rolling element bearings," *Sensors*, vol. 18, no. 5, Article ID 1466, 2018.
- [2] G. Yu, "A concentrated time-frequency analysis tool for bearing fault diagnosis," *IEEE Transactions on Instrumentation and Measurement*, vol. 69, no. 2, pp. 371–381, 2020.
- [3] S. N. Chegini, A. Bagheri, and F. Najafi, "Application of a new EWT-based denoising technique in bearing fault diagnosis," *Measurement*, vol. 144, pp. 275–297, 2019.
- [4] X. Wang, Y. Zi, and Z. He, "Multiwavelet denoising with improved neighboring coefficients for application on rolling bearing fault diagnosis," *Mechanical Systems and Signal Processing*, vol. 25, no. 1, pp. 285–304, 2011.
- [5] R. Abdelkader, A. Kaddour, and Z. Derouiche, "Enhancement of rolling bearing fault diagnosis based on improvement of empirical mode decomposition denoising method," *International Journal of Advanced Manufacturing Technology*, vol. 97, no. 5-8, pp. 3099–3117, 2018.
- [6] S. Zhang, Y. Wang, S. Jiang, and Z. Jiang, "Bearing fault diagnosis based on variational mode decomposition and total variation denoising," *Measurement Science and Technology*, vol. 27, no. 7, Article ID 075101, 2016.
- [7] J. Li, H. Wang, X. Wang, and Y. Zhang, "Rolling bearing fault diagnosis based on improved adaptive parameterless empirical wavelet transform and sparse denoising," *Measurement*, vol. 152, Article ID 107392, 2020.
- [8] Q. Xiong, Y. Xu, Y. Peng, W. Zhang, Y. Tang, and L. Tang, "Low-speed rolling bearing fault diagnosis based on EMD denoising and parameter estimate with alpha stable distribution," *Journal of Mechanical Science and Technology*, vol. 31, no. 4, pp. 1587–1601, 2017.
- [9] C. Ni, T. R. Lin, J. P. Xing, and J. Z. Xue, "A time-frequency analysis of non-stationary signals using variation mode decomposition and synchrosqueezing techniques," in *Proceedings of the Prognostics and System Health Management Conference (PHM-Qingdao)*, pp. 1–6, IEEE, Qingdao, China, October 2019.
- [10] Y. Peng, Z. Li, K. He et al., "Quality monitoring of aluminum alloy DPMIG welding based on broadband mode decomposition and MMC-FCH," *Measurement*, vol. 158, Article ID 107683, 2020.
- [11] Y. Peng, Z. Li, K. He, Y. Liu, Q. Li, and L. Liu, "Broadband mode decomposition and its application to the quality

- evaluation of welding inverter power source signals,” *IEEE Transactions on Industrial Electronics*, vol. 67, no. 11, p. 1, 2019.
- [12] K. Gupta and K. Raju, “Bearing fault analysis using variational mode decomposition,” in *Proceedings of the 9th International Conference on Industrial and Information Systems (ICIIS)*, pp. 1–6, IEEE, Gwalior, India, December 2014.
- [13] Q. Wang, L. Wang, H. Yu, D. Nandi, and A. K. Nandi, “Utilizing SVD and VMD for denoising non-stationary signals of roller bearings,” *Sensors*, vol. 22, no. 1, p. 195, 2021.
- [14] D. Zhen, J. Guo, Y. Xu, H. Gu, and F. Gu, “A novel fault detection method for rolling bearings based on non-stationary vibration signature analysis,” *Sensors*, vol. 19, no. 18, Article ID 3994, 2019.
- [15] Z. Wu and N. E. Huang, “Ensemble empirical mode decomposition: a noise-assisted data analysis method,” *Advances in Adaptive Data Analysis*, vol. 01, no. 01, pp. 1–41, 2009.
- [16] X. Xue, J. Zhou, Y. Xu, W. Li, and C. Li, “An adaptively fast ensemble empirical mode decomposition method and its applications to rolling element bearing fault diagnosis,” *Mechanical Systems and Signal Processing*, vol. 62–63, pp. 444–459, 2015.
- [17] L. Song, H. Chen, and P. Chen, “Vibration-based intelligent fault diagnosis for roller bearings in low-speed rotating machinery,” *IEEE Transactions on Instrumentation and Measurement*, vol. 67, no. 8, pp. 1887–1899, 2018.
- [18] T. Han, Q. Liu, and A. C. Tan, “Fault feature extraction of low speed roller bearing based on Teager energy operator and CEEMD,” *Measurement*, vol. 138, pp. 400–408, 2019.
- [19] Y. Jiao, G. Li, Z. Wu, H. Geng, J. Cheng, and L. Cheng, “Fault analysis for low-speed heavy-duty crane slewing bearing based on wavelet energy spectrum coefficient,” in *Advances in Acoustic Emission Technology*, pp. 63–74, Springer, Cham, 2017.
- [20] H. Cao, H. Shao, X. Zhong, Q. Deng, X. Xuan, and J. Xuan, “Unsupervised domain-share CNN for machine fault transfer diagnosis from steady speeds to time-varying speeds,” *Journal of Manufacturing Systems*, vol. 62, pp. 186–198, 2022.
- [21] T. Zhou and E. L. Droguett, “Towards trustworthy machine fault diagnosis: a probabilistic Bayesian deep learning framework,” *Reliability Engineering & System Safety*, vol. 224, Article ID 108525, 2022.
- [22] Z. C. Wang, Y. F. Peng, Y. F. Liu, K. F. He, Z. T. Wu, and B. Q. Li, “The calculation method of PV direct current energy based on modulated broadband mode decomposition and compound Simpson integral algorithm,” *IEEE Access*, vol. 9, pp. 51403–51415, 2021.
- [23] Y. Peng, J. Chen, Y. Liu et al., “Roller bearing fault diagnosis based on adaptive sparsest narrow-band decomposition and MMC-FCH,” *Shock and Vibration*, vol. 2019, pp. 1–17, 2019.
- [24] Y. Peng, J. Cheng, Y. Li, and B. Li, “Adaptive sparsest narrow-band decomposition method and its applications to rotor fault diagnosis,” *Measurement*, vol. 91, pp. 451–459, 2016.
- [25] M. N. A. H. Sha’abani, N. Fuad, N. Jamal, and E. M. N. E. M. Nasir, “Selection of intrinsic mode function in ensemble empirical mode decomposition based on peak frequency of PSD for EEG data analysis,” in *Proceedings of the Third International Conference on Trends in Computational and Cognitive Engineering*, pp. 213–221, Springer, Singapore, February 2022.
- [26] X. Song, Z. Liao, H. Wang, W. Chen, and P. Chen, “Incrementally accumulated holographic SDP characteristic fusion method in ship propulsion shaft bearing fault diagnosis,” *Measurement Science and Technology*, vol. 33, no. 4, Article ID 045011, 2022.
- [27] B. Pang, M. Nazari, Z. Sun, J. Li, and G. Tang, “An Optimized Variational Mode Extraction Method for Rolling Bearing Fault Diagnosis,” *Structural Health Monitoring*, vol. 21, no. 2, pp. 558–570, 2022.
- [28] T. Jin, C. Yan, C. Chen, Z. Yang, H. Tian, and J. Guo, “New domain adaptation method in shallow and deep layers of the CNN for bearing fault diagnosis under different working conditions,” *International Journal of Advanced Manufacturing Technology*, vol. 10, pp. 1–12, 2017.
- [29] H. Fan, S. Shao, X. Zhang, X. Wan, X. Ma, and H. Ma, “Intelligent fault diagnosis of rolling bearing using FCM clustering of EMD-PWVD vibration images,” *IEEE Access*, vol. 8, pp. 145194–145206, 2020.
- [30] I. Attoui, B. Oudjani, N. Boutasseta, N. Fergani, M. S. Bouakkaz, and A. Bouraiou, “Novel predictive features using a wrapper model for rolling bearing fault diagnosis based on vibration signal analysis,” *International Journal of Advanced Manufacturing Technology*, vol. 106, no. 7–8, pp. 3409–3435, 2020.
- [31] B. Li, R. Tong, J. Chi, and K. Chi, “Bearing fault diagnosis using synthetic quantitative index-based adaptive underdamped stochastic resonance,” *Mathematical Problems in Engineering*, vol. 2021, Article ID 8888079, 10 pages, 2021.